

## Canceling Out Intensity Mapping Foregrounds

Patrick C. Breysse<sup>1</sup>, Christopher J. Anderson<sup>2</sup>, and Philippe Berger<sup>3</sup>

<sup>1</sup>*Canadian Institute for Theoretical Astrophysics, University of Toronto,  
60 St. George Street, Toronto, Ontario M5S 3H8, Canada*

<sup>2</sup>*NASA Goddard Space Flight Center, Greenbelt, Maryland 20771, USA*

<sup>3</sup>*Jet Propulsion Laboratory, California Institute of Technology, 4800 Oak Grove Drive,  
M/S 169-237, Pasadena, California 91109, USA*

 (Received 25 July 2019; revised manuscript received 4 October 2019; published 4 December 2019)

Intensity mapping of the 21 cm line has arisen as a powerful probe of the high-redshift Universe, but its potential is limited by extremely bright foregrounds and high source confusion. We propose a new analysis which can help solve both problems. From the combination of an intensity map with an overlapping galaxy survey, we construct a new one-point statistic which is unbiased by foregrounds and contains information left out of conventional analyses. We show that our method can measure the HI mass function with unprecedented precision using observations similar to recent 21 cm detections.

DOI: [10.1103/PhysRevLett.123.231105](https://doi.org/10.1103/PhysRevLett.123.231105)

Many experiments are studying the evolution of the Universe with the redshifted 21 cm line [1–7], seeking to map vast swaths of cosmic history using line intensity mapping (LIM) [8–11]. Intensity maps do not resolve individual emitters but instead map fluctuations in the density of neutral hydrogen. This gives them sensitivity to the aggregate emission from all galaxies, as well as the neutral intergalactic medium. By targeting a narrow line, maps can be made in three dimensions by observation at different frequencies. LIM surveys can quickly map large volumes, allowing unprecedented constraints on fundamental cosmology [12–16]. They also provide information about faint objects below conventional detection thresholds. Theory predicts that the number of detected objects will be dwarfed by these systems, which accrete and merge to form galaxies such as our Milky Way [17].

Currently, the largest limiting factor in 21 cm cosmology comes from foregrounds which are typically orders of magnitude brighter than the signal [18–20]. These foregrounds have limited attempts to observe HI in autocorrelation. There have, however, been detections of cross spectra between HI maps and galaxy surveys, at redshift  $z \sim 0.08$  [21] with Parkes telescope data and the 2dF galaxy survey [22], and another at  $z \sim 0.8$  with Green Bank Telescope (GBT) data [23] and the WiggleZ survey [24]. Cross-correlation is robust against foreground contamination because galaxies and HI trace the same large-scale structure, while the foregrounds do not.

Even when detected, the signal is challenging to interpret. Intensity maps are typically analyzed using power spectra. A Gaussian density field is fully described by its power spectrum. However, 21 cm maps are highly non-Gaussian, as the HI distribution is determined by complex, nonlinear baryon dynamics.

For example, consider an experiment like Parkes-2dF or GBT-WiggleZ. At  $z < 1$ , virtually all HI is found within halos, and we can describe its distribution with the HI mass function (HIMF)  $\phi_{\text{HI}}(M_{\text{HI}})$ , which gives the number density of halos with a given HI mass. Let us consider a modified Schechter HIMF:

$$\phi(M_{\text{HI}}) = \ln(10)\phi_* \left(\frac{M_{\text{HI}}}{M_*}\right)^{1+\alpha} e^{-M_{\text{HI}}/M_* - M_{\text{min}}/M_{\text{HI}}}. \quad (1)$$

This basic form has been used many times in the literature [25–27]. We have added a low-mass cutoff at  $M_{\text{min}}$ , as intensity maps lack hard detection thresholds. Power spectra, sensitive only to Gaussian information, can access only the first two moments of the HIMF [28], while it would require four numbers,  $(\phi_*, M_*, \alpha, M_{\text{min}})$ , to fully determine Eq. (1). Furthermore, there are degeneracies between  $\phi_*$  and cosmological parameters that intensity maps might seek to measure, such as halo bias, the growth rate of fluctuations, and the amplitude of primordial non-Gaussianity [29–31].

It was suggested in Refs. [32,33] that this non-Gaussianity could be accessed using one-point statistics, as opposed to two-point statistics like power spectra.  $P(D)$  analysis, which has seen use for decades in many fields [34–39], allows mapping between the HIMF and the probability distribution function (PDF)  $\mathcal{P}(T)$  of voxel (or three-dimensional pixel) intensity  $T$ . This statistic, termed the voxel intensity distribution (VID), has been shown to significantly increase the information which can be gained from an intensity map [40].

Unfortunately, as with the autospectrum, the VID of a 21 cm map would be contaminated with unsubtracted foregrounds. Rather than expose ourselves to this large

potential source of bias, we introduce here a one-point analog to the cross spectrum, extending the VID formalism to remove foreground bias. We will then forecast how this technique can be applied to HI observations.

The approach we propose here relies on a simple fact: for independent random variables  $T_1$  and  $T_2$ , the PDF  $\mathcal{P}_{1+2}(T)$  of their sum  $T = T_1 + T_2$  is the *convolution* of their individual PDFs  $\mathcal{P}_1(T)$  and  $\mathcal{P}_2(T)$ . This is straightforward to prove. We can write

$$\mathcal{P}_{1+2}(T) = \iint \mathcal{P}_1(T')\mathcal{P}_2(T'')\delta_D(T-T'-T'')dT'dT'', \quad (2)$$

where  $\delta_D$  is a Dirac delta function. Evaluating one integral leaves a convolution,

$$\mathcal{P}_{1+2}(T) = \int \mathcal{P}_1(T')\mathcal{P}_2(T-T')dT' = (\mathcal{P}_1 \circ \mathcal{P}_2)(T). \quad (3)$$

We can make use of the Fourier convolution theorem to turn this into a product in Fourier space:

$$\tilde{\mathcal{P}}_{1+2}(\mathcal{T}) = \tilde{\mathcal{P}}_1(\mathcal{T})\tilde{\mathcal{P}}_2(\mathcal{T}), \quad (4)$$

where  $\mathcal{T} \equiv 2\pi/T$  is the Fourier conjugate of  $T$ , and  $\tilde{\mathcal{P}}(\mathcal{T})$  is the Fourier transform of  $\mathcal{P}(T)$  (also known as the characteristic function). In an intensity map, the observed  $T$  in a given voxel is the sum of a signal component  $T_S$  with PDF  $\mathcal{P}_S$  and a contribution from noise and foregrounds which we will abbreviate as  $T_{\text{FG}}$  with PDF  $\mathcal{P}_{\text{FG}}$ . The full VID of a map is then the convolution  $\mathcal{P}_S \circ \mathcal{P}_{\text{FG}}$ .

As stated above,  $\mathcal{P}_{\text{FG}}$  is hard to model to sufficient precision, so it will be difficult to apply the VID statistic directly to 21 cm data. We will therefore use a separate dataset with different systematics to isolate our signal. Assume that our volume contains both a 21 cm map and an optical galaxy survey. In each voxel, we know the total radio intensity  $T_S + T_{\text{FG}}$  and the number  $N_{\text{det}}$  of detected optical galaxies.  $T_S$  and  $N_{\text{det}}$  will be correlated, due both to the large-scale structure and the HI content of the optical galaxies. We can therefore construct *conditional* PDFs  $\mathcal{P}(T|N_{\text{det}})$ . We refer to these PDFs as conditional VIDs, or CVIDs.

Crucially, each CVID will be a convolution of a signal part, which depends on  $N_{\text{det}}$ , and a noise or foreground part, which does not. If we compare voxels with different  $N_{\text{det}}$ , we can write

$$\frac{\tilde{\mathcal{P}}(\mathcal{T}|N_{\text{det}}^1)}{\tilde{\mathcal{P}}(\mathcal{T}|N_{\text{det}}^2)} = \frac{\tilde{\mathcal{P}}_S(\mathcal{T}|N_{\text{det}}^1)\tilde{\mathcal{P}}_{\text{FG}}(\mathcal{T})}{\tilde{\mathcal{P}}_S(\mathcal{T}|N_{\text{det}}^2)\tilde{\mathcal{P}}_{\text{FG}}(\mathcal{T})} = \frac{\tilde{\mathcal{P}}_S(\mathcal{T}|N_{\text{det}}^1)}{\tilde{\mathcal{P}}_S(\mathcal{T}|N_{\text{det}}^2)}. \quad (5)$$

It is clear that the above ratio is *unbiased* by foregrounds, as the deconvolution cancels out the component which is common to both CVIDs.

In practice, we do not compute continuous PDFs directly from maps. Instead, we estimate PDFs using histograms  $B_i \approx \mathcal{P}(T_i)\Delta TN_{\text{vox}}$ , where  $B_i$  is the number of voxels in a bin of width  $\Delta T$  centered at  $T_i$ , and  $N_{\text{vox}}$  is the total number of voxels. If we separate our map by  $N_{\text{det}}$  values, compute histograms  $B_i^{N_{\text{det}}}$  from each part, and then compute their Fourier transforms  $\tilde{B}_i^{N_{\text{det}}} = \Delta T \sum_j B_j^{N_{\text{det}}} \exp(i\mathcal{T}_i T_j)$ , we can write down the CVID ratio (CVR),

$$\tilde{\mathcal{R}}_i^{N_{\text{det}}^1 N_{\text{det}}^2} = \frac{\tilde{B}_i^{N_{\text{det}}^1}}{\tilde{B}_i^{N_{\text{det}}^2}}. \quad (6)$$

It is easy to show that the expectation value of  $\tilde{\mathcal{R}}_i^{N_{\text{det}}^1 N_{\text{det}}^2}$  is proportional to the ratio from Eq. (5) and thus is unbiased by foregrounds.

Figure 1 shows an example of how this works. The left panel shows predicted histograms for a Parkes-2dF map with a Gaussian  $\mathcal{P}_{\text{FG}}$ , with the signal contribution computed as described below. The right panel shows the CVR computed *only from the signal*. Both panels include, for illustration, a toy data realization. If we assume that  $T_S$  and  $T_{\text{FG}}$  are independent draws from  $\mathcal{P}_S$  and  $\mathcal{P}_{\text{FG}}$ , then each  $B_i$  is an independent draw from a binomial distribution with mean  $\langle B_i \rangle$  and variance

$$\text{var}(B_i) = \langle B_i \rangle (1 - \langle B_i \rangle / N_{\text{vox}}) \approx \langle B_i \rangle. \quad (7)$$

Based on the nearly diagonal correlation matrices shown in Fig. 2 of Ref. [40], this approximation seems reasonable, at least at low signal to noise. We can therefore create a sample histogram by drawing randomly from binomial distributions. We leave detailed testing of this approximation to future work.

From our toy data, it is clear that the simulation, which includes foregrounds, gives the same CVR as the foreground-free theory. Though we used a Gaussian  $\mathcal{P}_{\text{FG}}$ , the same would hold for any general PDF. If we can estimate the error on  $B_i^{N_{\text{det}}}$ , either with Eq. (7) or with simulations, then we can propagate this error through to get the error on the CVR directly from the data. This has two important implications. First, it means that we do not need a model of the foregrounds to estimate errors on  $\tilde{\mathcal{R}}_i^{10}$ . Second, it accounts for instabilities which appear when the denominator of Eq. (6) approaches zero, as seen at high  $\mathcal{T}$  in Fig. 1. Though the measured CVR deviates significantly from the expectation, the large error bar means that these points get correspondingly little weight.

Because we defined the CVR in Fourier space, it is, in general, complex. Figure 1 shows only the real part, but the imaginary part carries a comparable amount of information. For our forecasts below, we use the full, complex CVR value and propagate the error from Eq. (7) through to compute the covariances of the real part, the imaginary part, and any correlation between the two.

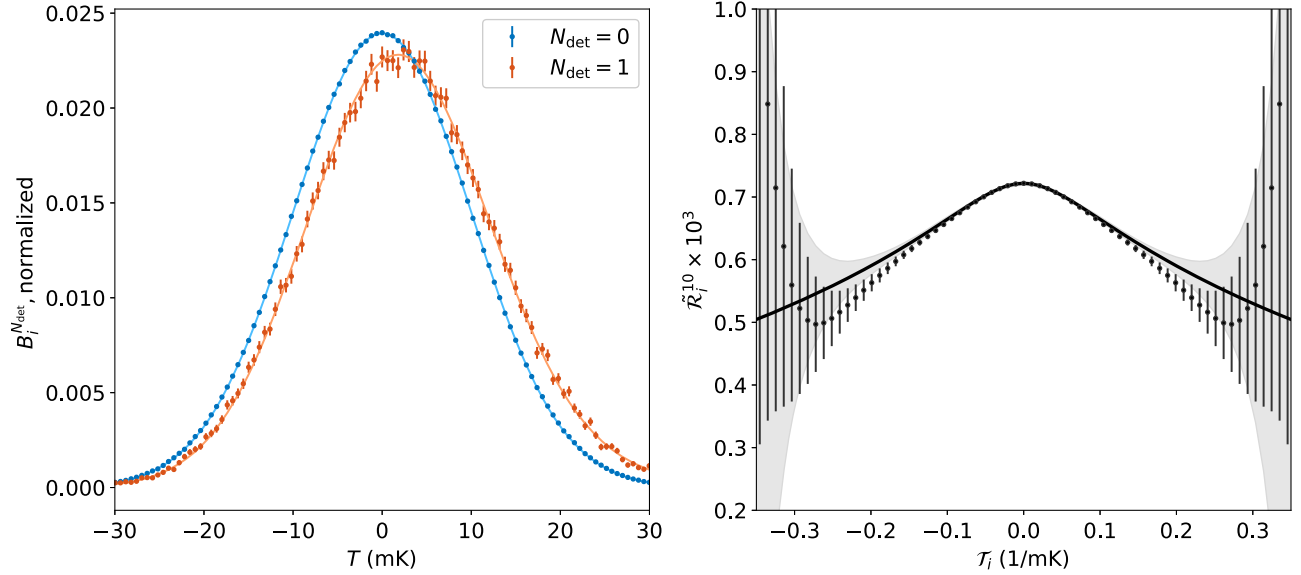


FIG. 1. Sample CVR analysis. (Left panel) Sample CVIDs for a model of Parkes-2dF data with noise and residual foregrounds modeled by a 10 mK Gaussian PDF, for voxels with  $N_{\text{det}} = 0$  (blue curve) and 1 (orange curve). Solid curves show the theoretical expectation, and points show a toy simulation as described in the text. Histograms are normalized to sum to unity. See below for details of the astrophysical modeling. (Right panel) CVR computed from the signal model only (solid curve) along with that estimated from the simulation. The gray band shows the predicted  $1\sigma$  error from the model. Note that CVR errors are highly correlated, leading to an offset at moderate  $T$ . Note also that we plot only the real part of the complex CVR.

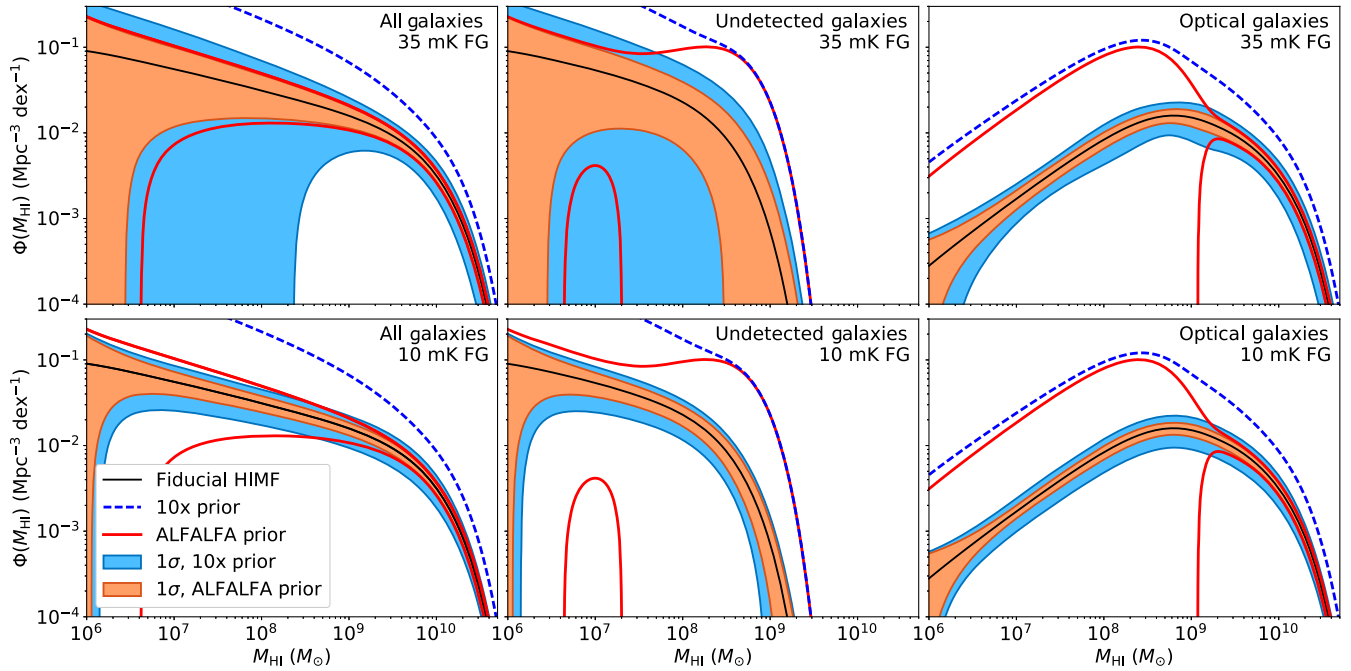


FIG. 2. (Left column) Forecasted CVR constraints on the HIMF of all galaxies, (center column) those undetected by the optical survey, and (right column) those detected optically. Black solid lines show our fiducial model [Eqs. (1), (9), and (10) with ALFALFA parameters], the other lines show  $1\sigma$  prior uncertainties for the ALFALFA priors (red solid) and the  $10\times$  ALFALFA priors (blue dashed). Shaded regions show the  $1\sigma$  regions after our Fisher forecast, both with the ALFALFA (red) and  $10\times$  ALFALFA priors (blue). The upper row shows the case with modest foreground cleaning ( $\sigma_{\text{FG}} = 35$  mK), the lower row the one with stronger cleaning ( $\sigma_{\text{FG}} = 10$  mK).

Now we need to connect the CVR to the HIMF. We can relate the two using a modified  $P(D)$  analysis [33,37,41]. In the standard  $P(D)$  case, we parametrize the source luminosity function, then assume some model for the number count PDF to predict  $\mathcal{P}(T)$ . We make two modifications here. First, we separate the population into line emitters which are associated 1:1 with optical galaxies and those which are not, giving two separate HIMFs which we will refer to with subscripts “det” and “un,” respectively. Second, we model how the counts of undetected galaxies depend on the presence of detected galaxies. We now present the detailed computation.

In each voxel, there are  $N_{\text{det}}$  detected optical galaxies and an unknown number  $N_{\text{un}}$  of unresolved HI emitters, so,

$$\tilde{\mathcal{P}}(T|N_{\text{det}}) = \tilde{\mathcal{P}}_{\text{det}}(T|N_{\text{det}})\tilde{\mathcal{P}}_{\text{un}}(T|N_{\text{det}}). \quad (8)$$

To compute  $\tilde{\mathcal{P}}_{\text{det}}$  and  $\tilde{\mathcal{P}}_{\text{un}}$ , we need separate HIMFs for the detected and undetected galaxy populations. For now, we assume an exponential separation,

$$\phi_{\text{un}}(M_{\text{HI}}) = \phi(M_{\text{HI}})e^{-M_{\text{HI}}/M_{\text{cut}}}, \quad (9)$$

$$\phi_{\text{det}}(M_{\text{HI}}) = \phi(M_{\text{HI}})(1 - e^{-M_{\text{HI}}/M_{\text{cut}}}), \quad (10)$$

with free parameter  $M_{\text{cut}}$ .

If  $N_{\text{det}} = 0$ , there is no contribution from detected galaxies and  $\mathcal{P}_{\text{det}}(T|0) = \delta_D(T)$ . If  $N_{\text{det}} = 1$ , then  $\mathcal{P}_{\text{det}}(T|1)$  is proportional to  $\phi_{\text{det}}$ , with appropriate normalization (see Ref. [33] for details). For higher values of  $N_{\text{det}}$ , we can recursively apply Eq. (4) to get

$$\tilde{\mathcal{P}}_{\text{det}}(T|N_{\text{det}}) = [\tilde{\mathcal{P}}_{\text{det}}(T|N_{\text{det}} = 1)]^{N_{\text{det}}}. \quad (11)$$

Note that in Eq. (11) we have implicitly assumed that the HIMF in a voxel is independent of how many galaxies it contains. This is known to be inaccurate, as more massive objects will be more strongly biased, shifting the HIMF to larger masses in dense voxels. Accurately modeling this effect will likely require simulations, so we neglect it for now.

For undetected galaxies, we do not know the value of  $N_{\text{un}}$ , so we have

$$\tilde{\mathcal{P}}_{\text{un}}(T|N_{\text{det}}) = \sum_{N_{\text{un}}} [\tilde{\mathcal{P}}_{\text{un}}(T|N_{\text{un}} = 1)]^{N_{\text{un}}} \mathcal{P}(N_{\text{un}}|N_{\text{det}}), \quad (12)$$

where  $\mathcal{P}_{\text{un}}(T|N_{\text{un}} = 1)$  is proportional to  $\phi_{\text{un}}$ , and  $\mathcal{P}(N_{\text{un}}|N_{\text{det}})$  describes the correlation between optical galaxies and unresolved HI emitters. If there is no clustering,  $\mathcal{P}_{\text{un}}$  has no dependence on  $N_{\text{det}}$  and will cancel out of the CVR. However, we know that HI and optical galaxies should be at least somewhat correlated, though that correlation may be color and scale dependent [21,42,43]. We will model the number of detected and undetected galaxies at each voxel as independent draws from two

Poisson distributions. To include clustering, the means  $\mu_{\text{un}}$  and  $\mu_{\text{det}}$  of the detected and undetected galaxy counts are drawn from a log-normal distribution and are 100% correlated at each voxel.

Galaxy count distributions are known to be reasonably approximated by log-normal PDFs [44,45],

$$\mathcal{P}_{\text{LN}}(\mu_{\text{det}}) = \frac{1}{\mu_{\text{det}} \sqrt{2\pi\sigma_G^2}} \times \exp \left\{ -\frac{1}{2\sigma_G^2} \left[ \ln \left( \frac{\mu_{\text{det}}}{\bar{N}_{\text{det}}} \right) + \frac{\sigma_G^2}{2} \right]^2 \right\}, \quad (13)$$

where the  $\sigma_G$  parameter represents the effect of clustering. In the limit in which  $\sigma_G \sim 0$ ,  $\mathcal{P}_{\text{LN}}(\mu_{\text{det}})$  tends to a  $\delta$  function centered at  $\bar{N}_{\text{det}}$ , and there is no effect from clustering.

Since we are assuming that  $\mu_{\text{un}}$  and  $\mu_{\text{det}}$  are fully correlated, we take  $\mu_{\text{un}} = f_{\text{un}}\mu_{\text{det}}$  in every voxel, where  $f_{\text{un}} \equiv \bar{N}_{\text{un}}/\bar{N}_{\text{det}}$ . We then can write

$$\mathcal{P}(N_{\text{un}}|N_{\text{det}}) = \int \mathcal{P}(N_{\text{un}}|f_{\text{un}}\mu_{\text{det}}) \mathcal{P}(\mu_{\text{det}}|N_{\text{det}}) d\mu_{\text{det}}. \quad (14)$$

We can use Bayes’s theorem to state that

$$\mathcal{P}(\mu_{\text{det}}|N_{\text{det}}) \propto \mathcal{P}(N_{\text{det}}|\mu_{\text{det}}) \mathcal{P}_{\text{LN}}(\mu_{\text{det}}), \quad (15)$$

where  $\mathcal{P}_{\text{LN}}$  acts as our “prior.” With our assumption of Poisson statistics, we have

$$\mathcal{P}(N_{\text{un}}|N_{\text{det}}) \propto \int \mathcal{P}_{\text{Pois}}(N_{\text{un}}|f_{\text{un}}\mu_{\text{det}}) \mathcal{P}_{\text{LN}}(\mu_{\text{det}}) \times \mathcal{P}_{\text{Pois}}(N_{\text{det}}|\mu_{\text{det}}) d\mu_{\text{det}}, \quad (16)$$

where  $\mathcal{P}_{\text{Pois}}(N|\mu)$  is the Poisson distribution with mean  $\mu$ .

We can now predict a CVR from our HIMF model. We will now examine what information could be gained from such an analysis. Consider a model of the Parkes-2dF maps described in Ref. [21], with free parameters  $(\phi_*, M_*, \alpha, M_{\text{min}}, M_{\text{cut}}, \sigma_G)$ . Assume that HI evolves negligibly from  $z = 0-0.05$ , and use the best-fit HIMF from ALFALFA [27] as a model, with  $\phi_* = (4.5 \pm 0.8) \times 10^{-3} \text{ Mpc}^{-3} \text{ dex}^{-1}$ ,  $\log(M_*/M_{\odot}) = 9.94 \pm 0.05$ , and  $\alpha = -1.25 \pm 0.1$ . We arbitrarily choose  $M_{\text{min}} = 10^5 M_{\odot}$  so that it falls below the ALFALFA detection threshold, and  $M_{\text{cut}} = 3 \times 10^8 M_{\odot}$  to get the correct number of detected galaxies [22]. We compute  $\sigma_G$  following Ref. [33]. Note that we assume the same value for  $\phi_*$  and  $\alpha$  for both the detected and undetected populations.

We assume a Gaussian  $\mathcal{P}_{\text{FG}}$  but note again that this procedure would work regardless of the assumed form. Based on a cursory examination of the cleaned Parkes maps shown in Fig. 1 of Ref. [21], we set  $\sigma_{\text{FG}} = 10 \text{ mK}$ . However, in the process of cleaning the maps to this level, it is possible that some of the signal would be removed. The simplest response to this would be to use maps which have



not been cleaned as aggressively. We will roughly model this case with a second model where we somewhat arbitrarily choose  $\sigma_{\text{FG}} = 35$  mK. This should give an impression of how our results scale with foreground contamination.

We can forecast constraints on our model using the Fisher matrix formalism [46,47]. We consider only  $N_{\text{det}} = 0$  and 1 here, as few data voxels have  $N_{\text{det}} > 1$ . As we neglect evolution from the  $z = 0$  ALFALFA galaxies, we can use their quoted systematic errors as priors on  $\phi_*$ ,  $M_*$ , and  $\alpha$ . Many LIM surveys, including the GBT-WiggleZ survey, target higher redshifts where we cannot neglect the HIMF evolution. This means that we would not be able to use the high-quality  $z = 0$  priors. For simplicity, we will not attempt to directly model this evolution here, but we will very roughly approximate it by adopting a second, weaker set of priors. If we compare HI measurements from damped Lyman- $\alpha$  absorbers at redshifts  $\sim 0$  and  $\sim 1$ , we see that the  $z \sim 1$  measurements are an order of magnitude or so worse (see Figs. 2 and 3 of Ref. [48]). We therefore choose our second set of priors to be 10 times worse than ALFALFA. In both cases, we assume 10% prior knowledge of  $\sigma_G$ , which would have to come from simulations, and uninformative fractional priors of 10 on both  $M_{\text{cut}}$  and  $M_{\text{min}}$ . We assume a cosmology consistent with the Planck 2015 results [49].

Figure 2 shows the results of our Fisher forecasts. We plot  $1\sigma$  confidence intervals around our fiducial models for the total, detected, and undetected populations. Even in the most pessimistic case, with strong foregrounds and weak ( $10\times$  ALFALFA) priors, we get a good measurement of the bright end of the HIMF and the detected galaxy HIMF. If we know enough to trust the strong ALFALFA priors, then the CVID adds important constraints on the HIMF of the optical galaxies and a modest measurement of that of the unresolved galaxies, both of which cannot be obtained from ALFALFA alone. With 10 mK foregrounds, the CVID dramatically improves on the priors. The very brightest end of the HIMF is still dominated by ALFALFA, but the CVID has added a wealth of information about faint galaxies which cannot be obtained conventionally. Unfortunately, even the intensity mapping data lose sensitivity at the very faintest end of the HIMF. Even stronger foreground cleaning would be needed to measure  $M_{\text{min}}$ .

These forecasts clearly demonstrate the utility of this method. However, we have made a number of assumptions that deserve further study. The log-normal galaxy count PDF is likely overly simplistic, and it could be replaced by a more sophisticated prescription [50]. In Eqs. (9) and (10), we assumed that optical galaxies host the brightest 21 cm emitters. This should hold for blue, gas-rich galaxies, but a number of bright optical galaxies are red and gas poor [51] and therefore have weaker HI emission. As mentioned above, we have entirely neglected luminosity-dependent bias in our forecasting. Though Parkes and GBT are single dish, many 21 cm experiments are interferometric. We

compute CVIDs from real-space maps, while interferometers natively observe the sky in Fourier space. The process of inverse Fourier transforming a map will induce pixel-to-pixel covariances. In principle, it should be possible to model this effect since the Fourier space coverage of the interferometer is known, but it would require additional care. Finally, we assumed that we can apply some degree of foreground cleaning to our data without affecting our signal. In the Parkes foreground cleaning, the signal was suppressed along with the foregrounds [21], which if uncorrected would bias our CVR measurements. These caveats motivate additional study of this method using mock datasets, as in Ref. [40].

Speaking broadly, we expect this new technique to share many of the benefits and limitations of standard cross spectra. Reference [40] found that the VID and autospectrum contain comparable and complementary amounts of information. It is reasonable to expect qualitatively similar results here, that the cross spectrum and CVID would have similar “detection significance,” though we leave rigorous study of the combination of these two statistics for future work.

Though we have focused here on a simple HIMF fit, the potential utility of this method extends much further. Given a large enough sample of cross-correlation galaxies, one could separate out galaxies with different properties, for example, to see how the HIMF varies with optical luminosity or galaxy color [21,52]. With intensity maps of other lines [53–63], one could, for example, measure molecular gas in Lyman- $\alpha$  emitters [64], or study active galactic nuclei feedback [65]. The CVR can also be modified to combine intensity maps of different lines [28,66–68]. In this case, one would use the PDF  $\mathcal{P}(T_1|T_2)$  for line intensities  $T_1$  and  $T_2$ . As  $T_2$  would be a continuous variable, rather than the binary integer we conditioned on above, the CVR estimator would need to be modified.

Cross-correlations have long been a powerful cosmological tool, and they will only become more critical as more intensity mapping surveys come on line. With this Letter, we have demonstrated a one-point cross-correlation method that can be used to clean foregrounds and probe astrophysics inaccessible to conventional surveys. With some refinement, this will be a valuable tool for many future experiments.

The authors would like to thank Ue-Li Pen and Hamsa Padmanabhan for the useful conversations. P. B. was supported by Jet Propulsion Laboratory, California Institute of Technology, under a contract with the National Aeronautics and Space Administration.

- 
- [1] S. J. Tingay, R. Goetze, J. D. Bowman, D. Emrich, S. M. Ord, D. A. Mitchell, M. F. Morales, T. Booler, B. Crosse, R. B. Wayth *et al.*, *Pub. Astron. Soc. Aust.* **30**, e007 (2013).

- [2] M. P. van Haarlem, M. W. Wise, A. W. Gunst, G. Heald, J. P. McKean, J. W. T. Hessels, A. G. de Bruyn, R. Nijboer, J. Swinbank, R. Fallows *et al.*, *Astron. Astrophys.* **556**, A2 (2013).
- [3] K. Bandura, G. E. Addison, M. Amiri, J. R. Bond, D. Campbell-Wilson, L. Connor, J.-F. Cliche, G. Davis, M. Deng, N. Denman *et al.*, *Proc. SPIE Int. Soc. Opt. Eng.* **9145**, 22 (2014).
- [4] Z. S. Ali, A. R. Parsons, H. Zheng, J. C. Pober, A. Liu, J. E. Aguirre, R. F. Bradley, G. Bernardi, C. L. Carilli, C. Cheng *et al.*, *Astrophys. J.* **809**, 61 (2015).
- [5] Y. Xu, X. Wang, and X. Chen, *Astrophys. J.* **798**, 40 (2015).
- [6] L. B. Newburgh, K. Bandura, M. A. Bucher, T.-C. Chang, H. C. Chiang, J. F. Cliche, R. Davé, M. Dobbs, C. Clarkson, K. M. Ganga *et al.*, *Proc. SPIE Int. Soc. Opt. Eng.* **9906**, 99065X (2016).
- [7] D. R. DeBoer, A. R. Parsons, J. E. Aguirre, P. Alexander, Z. S. Ali, A. P. Beardsley, G. Bernardi, J. D. Bowman, R. F. Bradley, C. L. Carilli *et al.*, *Publ. Astron. Soc. Pac.* **129**, 045001 (2017).
- [8] M. Suginoara, T. Suginoara, and D. N. Spergel, *Astrophys. J.* **512**, 547 (1999).
- [9] M. F. Morales and J. S. B. Wyithe, *Annu. Rev. Astron. Astrophys.* **48**, 127 (2010).
- [10] J. R. Pritchard and A. Loeb, *Rep. Prog. Phys.* **75**, 086901 (2012).
- [11] E. D. Kovetz, M. P. Viero, A. Lidz, L. Newburgh, M. Rahman, E. Switzer, M. Kamionkowski, J. Aguirre, M. Alvarez, J. Bock *et al.*, [arXiv:1709.09066](https://arxiv.org/abs/1709.09066).
- [12] J. R. Shaw, K. Sigurdson, M. Sitwell, A. Stebbins, and U.-L. Pen, *Phys. Rev. D* **91**, 083514 (2015).
- [13] A. Liu, J. R. Pritchard, R. Allison, A. R. Parsons, U. Seljak, and B. D. Sherwin, *Phys. Rev. D* **93**, 043013 (2016).
- [14] A. Ewall-Wice, J. Hewitt, A. Mesinger, J. S. Dillon, A. Liu, and J. Pober, *Mon. Not. R. Astron. Soc.* **458**, 2710 (2016).
- [15] A. Liu and A. R. Parsons, *Mon. Not. R. Astron. Soc.* **457**, 1864 (2016).
- [16] S. Foreman, P. D. Meerburg, A. van Engelen, and J. Meyers, *J. Cosmol. Astropart. Phys.* **07** (2018) 046.
- [17] R. S. Somerville and R. Davé, *Annu. Rev. Astron. Astrophys.* **53**, 51 (2015).
- [18] S. P. Oh and K. J. Mack, *Mon. Not. R. Astron. Soc.* **346**, 456 (2003).
- [19] X. Wang, M. Tegmark, M. G. Santos, and L. Knox, *Astrophys. J.* **650**, 529 (2006).
- [20] A. Liu and M. Tegmark, *Phys. Rev. D* **83**, 103006 (2011).
- [21] C. J. Anderson, N. J. Luciw, Y. C. Li, C. Y. Kuo, J. Yadav, K. W. Masui, T. C. Chang, X. Chen, N. Oppermann, Y. W. Liao *et al.*, *Mon. Not. R. Astron. Soc.* **476**, 3382 (2018).
- [22] M. Colless, G. Dalton, S. Maddox, W. Sutherland, P. Norberg, S. Cole, J. Bland-Hawthorn, T. Bridges, R. Cannon, C. Collins *et al.*, *Mon. Not. R. Astron. Soc.* **328**, 1039 (2001).
- [23] K. W. Masui, E. R. Switzer, N. Banavar, K. Bandura, C. Blake, L.-M. Calin, T.-C. Chang, X. Chen, Y.-C. Li, Y.-W. Liao *et al.*, *Astrophys. J. Lett.* **763**, L20 (2013).
- [24] D. Parkinson, S. Riemer-Sørensen, C. Blake, G. B. Poole, T. M. Davis, S. Brough, M. Colless, C. Contreras, W. Couch, S. Croom *et al.*, *Phys. Rev. D* **86**, 103518 (2012).
- [25] P. Schechter, *Astrophys. J.* **203**, 297 (1976).
- [26] M. A. Zwaan, M. J. Meyer, L. Staveley-Smith, and R. L. Webster, *Mon. Not. R. Astron. Soc.* **359**, L30 (2005).
- [27] M. G. Jones, M. P. Haynes, R. Giovanelli, and C. Moorman, *Mon. Not. R. Astron. Soc.* **477**, 2 (2018).
- [28] A. Lidz, S. R. Furlanetto, S. P. Oh, J. Aguirre, T.-C. Chang, O. Doré, and J. R. Pritchard, *Astrophys. J.* **741**, 70 (2011).
- [29] A. Obuljen, E. Castorina, F. Villaescusa-Navarro, and M. Viel, *J. Cosmol. Astropart. Phys.* **05** (2018) 004.
- [30] S.-F. Chen, E. Castorina, M. White, and A. Slosar, *J. Cosmol. Astropart. Phys.* **07** (2019) 023.
- [31] E. Castorina and M. White, *J. Cosmol. Astropart. Phys.* **06** (2019) 025.
- [32] P. C. Breysse, E. D. Kovetz, and M. Kamionkowski, *Mon. Not. R. Astron. Soc.* **457**, L127 (2016).
- [33] P. C. Breysse, E. D. Kovetz, P. S. Behroozi, L. Dai, and M. Kamionkowski, *Mon. Not. R. Astron. Soc.* **467**, 2996 (2017).
- [34] P. A. G. Scheuer, *Proc. Cambridge Philos. Soc.* **53**, 764 (1957).
- [35] X. Barcons, G. B. Raymont, R. S. Warwick, A. C. Fabian, K. O. Mason, I. McHardy, and M. Rowan-Robinson, *Mon. Not. R. Astron. Soc.* **268**, 833 (1994).
- [36] D. Windridge and S. Phillipps, *Mon. Not. R. Astron. Soc.* **319**, 591 (2000).
- [37] S. K. Lee, S. Ando, and M. Kamionkowski, *J. Cosmol. Astropart. Phys.* **07** (2009) 007.
- [38] G. Patanchon, P. A. R. Ade, J. J. Bock, E. L. Chapin, M. J. Devlin, S. R. Dicker, M. Griffin, J. O. Gundersen, M. Halpern, P. C. Hargrave *et al.*, *Astrophys. J.* **707**, 1750 (2009).
- [39] J. Glenn, A. Conley, M. Béthermin, B. Altieri, A. Amblard, V. Arumugam, H. Aussel, T. Babbedge, A. Blain, J. Bock *et al.*, *Mon. Not. R. Astron. Soc.* **409**, 109 (2010).
- [40] H. T. Ihle, D. Chung, G. Stein, M. Alvarez, J. R. Bond, P. C. Breysse, K. A. Cleary, H. K. Eriksen, M. K. Foss, J. O. Gundersen *et al.*, *Astrophys. J.* **871**, 75 (2019).
- [41] S. Chen, J. T. L. Zwart, and M. G. Santos, [arXiv:1709.04045](https://arxiv.org/abs/1709.04045).
- [42] K. M. Hess and E. M. Wilcots, *Astron. J.* **146**, 124 (2013).
- [43] E. Papastergis, R. Giovanelli, M. P. Haynes, A. Rodríguez-Puebla, and M. G. Jones, *Astrophys. J.* **776**, 43 (2013).
- [44] P. Coles and B. Jones, *Mon. Not. R. Astron. Soc.* **248**, 1 (1991).
- [45] I. Kayo, A. Taruya, and Y. Suto, *Astrophys. J.* **561**, 22 (2001).
- [46] R. A. Fisher, *J. R. Stat. Soc.* **98**, 39 (1935).
- [47] M. Tegmark, A. N. Taylor, and A. F. Heavens, *Astrophys. J.* **480**, 22 (1997).
- [48] H. Padmanabhan, A. Refregier, and A. Amara, *Mon. Not. R. Astron. Soc.* **469**, 2323 (2017).
- [49] R. Adam, P. A. R. Ade, N. Aghanim, Y. Akrami, M. I. R. Alves, F. Argüeso, M. Arnaud, F. Arroja, M. Ashdown *et al.* (Planck Collaboration), *Astron. Astrophys.* **594**, A1 (2016).
- [50] O. Leicht, C. Uhlemann, F. Villaescusa-Navarro, S. Codis, L. Hernquist, and S. Genel, *Mon. Not. R. Astron. Soc.* **484**, 269 (2019).
- [51] S. Cole, W. J. Percival, J. A. Peacock, P. Norberg, C. M. Baugh, C. S. Frenk, I. Baldry, J. Bland-Hawthorn, T. Bridges, R. Cannon *et al.*, *Mon. Not. R. Astron. Soc.* **362**, 505 (2005).

- [52] L. Wolz, C. Blake, and J. S. B. Wyithe, *Mon. Not. R. Astron. Soc.* **470**, 3220 (2017).
- [53] E. Kovetz, P. C. Breyse, A. Lidz, J. Bock, C. M. Bradford, T.-C. Chang, S. Foreman, H. Padmanabhan, A. Pullen, and D. Riechers, *Bull. Am. Astron. Soc.* **51**, 101 (2019).
- [54] A. T. Crites, J. J. Bock, C. M. Bradford, T. C. Chang, A. R. Cooray, L. Duband, Y. Gong, S. Hailey-Dunsheath, J. Hunacek, and P. M. Koch, in *Millimeter, Submillimeter, and Far-Infrared Detectors and Instrumentation for Astronomy VII*, SPIE Proceedings Vol. 9153 (SPIE—International Society for Optical Engineering, Bellingham, WA, 2014), p. 91531W.
- [55] G. K. Keating, D. P. Marrone, G. C. Bower, E. Leitch, J. E. Carlstrom, and D. R. DeBoer, *Astrophys. J.* **830**, 34 (2016).
- [56] T. Y. Li, R. H. Wechsler, K. Devaraj, and S. E. Church, *Astrophys. J.* **817**, 169 (2016).
- [57] Y. Gong, A. Cooray, M. B. Silva, M. Zemcov, C. Feng, M. G. Santos, O. Dore, and X. Chen, *Astrophys. J.* **835**, 273 (2017).
- [58] R. A. C. Croft, J. Miralda-Escudé, Z. Zheng, M. Blomqvist, and M. Pieri, *Mon. Not. R. Astron. Soc.* **481**, 1320 (2018).
- [59] OST Mission Concept Study Team, arXiv:1809.09702.
- [60] H. Padmanabhan, *Mon. Not. R. Astron. Soc.* **488**, 3014 (2019).
- [61] G. J. Stacey, M. Aravena, K. Basu, N. Battaglia, B. Beringue, F. Bertoldi, J. R. Bond, P. Breyse, R. Bustos, and S. Chapman, in *Ground-Based and Airborne Telescopes VII*, SPIE Proceedings Vol. 10700 (SPIE—International Society for Optical Engineering, Bellingham, WA, 2018), p. 107001M.
- [62] A. Cooray, T.-C. Chang, S. Unwin, M. Zemcov, A. Coffey, P. Morrissey, N. Raouf, S. Lipsy, M. Shannon, and G. Wu, arXiv:1903.03144.
- [63] S. Dumitru, G. Kulkarni, G. Lagache, and M. G. Haehnelt, *Mon. Not. R. Astron. Soc.* **485**, 3486 (2019).
- [64] D. T. Chung, M. P. Viero, S. E. Church, R. H. Wechsler, M. A. Alvarez, J. R. Bond, P. C. Breyse, K. A. Cleary, H. K. Eriksen, M. K. Foss *et al.*, *Astrophys. J.* **872**, 186 (2019).
- [65] P. C. Breyse and R. M. Alexandroff, *Mon. Not. R. Astron. Soc.* **490**, 260 (2019).
- [66] P. C. Breyse and M. Rahman, *Mon. Not. R. Astron. Soc.* **468**, 741 (2017).
- [67] J. Fonseca, R. Maartens, and M. G. Santos, *Mon. Not. R. Astron. Soc.* **479**, 3490 (2018).
- [68] A. Beane, F. Villaescusa-Navarro, and A. Lidz, *Astrophys. J.* **874**, 133 (2019).